CANCER

A dual role for PSIP1/LEDGF in T cell acute lymphoblastic leukemia

Lisa Demoen[1,2], Filip Matthijssens[1,2], Lindy Reunes[1,2], Bruno Palhais[1,2], Béatrice Lintermans[1,2], Sara T'Sas[2,3], Igor Fijalkowski[2,4], Joachim Taminau[2,5], Muluembet Z. Akele[6], Siska Van Belle[6], Tom Taghon[2,7], Dieter Deforce[8], Filip Van Nieuwerburgh[8], Geert Berx[2,5], Panagiotis Ntziachristos[2,4], Zeger Debyser[6], Kaat Durinck[2,9], Tim Pieters[1,2,3,4]†, Steven Goossens[2,3]*†, Pieter Van Vlierberghe[1,2]†

T cell acute lymphoblastic leukemia (T-ALL) is an aggressive hematological malignancy. Current intensified therapeutic protocols coincide with severe side effects, and no salvage therapy is available for primary therapy-resistant or relapsed patients. This highlights the need to identify new therapeutic targets in T-ALL. PSIP1, dispensable for normal hematopoiesis, is a dependency factor in *KMT2A*-rearranged myeloid leukemia. Nonetheless, loss-of-function mutations suggest a tumor suppressor role for PSIP1 in T-ALL. Here, we demonstrate that the loss of *Psip1* accelerates T-ALL initiation in mice which we correlated with reduced H3K27me3 binding. Contrastingly, loss of PSIP1 impaired cell proliferation in several T-ALL cell lines. In cell lines, PSIP1 down-regulation leads to a reduction of COX20, an assembly factor of the cytochrome c oxidase in the mitochondria, and to a reduction in mitochondrial respiration. This indicates that PSIP1 can exert a dual role in the context of T-ALL, either as a tumor suppressor gene during tumor initiation or as a dependency factor in tumor maintenance.

INTRODUCTION

T cell acute lymphoblastic leukemia (T-ALL) is a rare, aggressive hematological malignancy characterized by a diffuse infiltration of the bone marrow by malignant T cell progenitors. They represent 10 to 15% of the pediatric and 25% of the adult acute lymphoblastic leukemia patients (*1*, *2*). The prognosis for patients with T-ALL has significantly improved with the introduction of intensified chemotherapy. Modern protocols reach cure rates of more than 80% in children and about 50% in adults (*1*, *3*). Nonetheless, intensified chemotherapy coincides with severe short- and long-term side effects. In addition, the outcome for primary therapy-resistant or relapse patients remains extremely poor. Therefore, there is an urgent need for a better molecular understanding of the pathogenesis to identify key drivers and therapeutic targets to develop more effective and less toxic therapeutic strategies.

PSIP1, also known as Lens epithelium derived growth factor (LEDGF), is an epigenetic reader of H3K36 di- and trimethylation marks that preferentially associates with actively transcribed chromatin (*4*). Two isoforms of PSIP1/LEDGF have been described, p75 and p52, which both contain the H3K36me2/3 binding PWWP domain. The smaller isoform, PSIP1/LEDFGF/p52, produced by alternative splicing, lacks the C-terminal protein-interacting integrase binding domain (*5*). PSIP1/LEDGF/p75 was demonstrated to be a critical component of the ternary PSIP1-KMT2A-Menin complex, with histone methyltransferase KMT2A, also known as MLL, as a component for transcriptional activation, while Menin functions as a critical molecular adaptor between the two proteins (*6*, *7*). *KMT2A* chromosomal rearrangements (KMT2Ar) are detected in 5 to 10% of the acute myeloid leukemia (AML) cases and in 3.3% of the T-ALL cases (*8*, *9*). More than 80 different fusion partners have been identified, which lead to epigenetic changes and consequently to transcriptional deregulation of essential hematopoietic regulatory networks, including *MEIS1* and *HOXA* genes (*10*–*12*). Menin, encoded by the *MEN1* gene, has been described both as a dependency factor in KMT2Ar leukemias (*13*) and as a key tumor suppressor in type 1 endocrine neoplasias (*14*). In these endocrine tumors, Menin regulates cell type–specific transcriptional programs by linking chromatin regulatory complexes such as KMT2A and KMT2D to specific target genes. In the context of AML, the interaction of PSIP1 with the N-terminal part of the KTM2Ar fusion oncogenes is essential for KMT2Ar-induced leukemic transformation (*13*, *15*–*18*). Noteworthy, a divergent effect was observed upon PSIP1 knockdown on wild-type (WT) KMT2A compared to the KMT2Ar fusion proteins. Depletion of PSIP1 expression reduced the occupancy of WT KMT2A at target genes and paradoxically increased the occupancy of KMT2Ar at these sites, suggesting a competition for the binding to these sites by WT KMT2A. However, KMT2Ar requires PSIP1 to recruit high-order protein complexes, which contain transcription elongation factors (*6*). Thus, although PSIP1 is unnecessary for the chromatin occupancy of KMT2Ar fusion proteins, it is essential for their leukemogenic activity. Furthermore, we previously demonstrated that PSIP1 is dispensable for steady-state hematopoiesis, making it an interesting therapeutic target in KTM2Ar AML (*18*).

Here, we investigated the role of PSIP1 in the initiation and maintenance of T-ALL. On the basis of inactivating *PSIP1* mutations and

[1]Lab of Normal and Malignant Hematopoiesis, Center for Medical Genetics, Department of Biomolecular Medicine, Ghent University, 9000 Ghent, Belgium. [2]Cancer Research Institute Ghent (CRIG), Ghent University, 9000 Ghent, Belgium. [3]Unit for Translational Research in Oncology, Department of Diagnostic Sciences, Ghent University, 9000 Ghent, Belgium. [4]Leukemia Therapy Resistance Laboratory, Center for Medical Genetics, Department of Biomolecular Medicine, Ghent University, 9000 Ghent, Belgium. [5]Department Biomedical Molecular Biology, 9000 Ghent University, Ghent, Belgium. [6]Laboratory for Molecular Virology and Gene Therapy, Department of Pharmaceutical and Pharmacological Sciences, Katholieke Universiteit (KU) Leuven, 3000 Leuven, Belgium. [7]T Cell Team Taghon, Department of Diagnostic Sciences, Ghent University, 9000 Ghent, Belgium. [8]Laboratory of Pharmaceutical Biotechnology, Ghent University, 9000 Ghent, Belgium. [9]Pediatric Precision Oncology Lab, Center for Medical Genetics, Department of Biomolecular Medicine, Ghent University, 9000 Ghent, Belgium.
*Corresponding author. Email: steven.goossens@ugent.be
†These authors contributed equally to this work.

reduced *PSIP1* level in patients with T-ALL, we postulated a tumor suppressor role for PSIP1. By knocking out *Psip1* in two spontaneous T-ALL mouse models, we demonstrated that loss of *Psip1* accelerates T-ALL formation, which is correlated with altered H3K27me3 signaling. On the basis of this, we propose a tumor-suppressive role for PSIP1 in T-ALL initiation. In contrast, depletion of PSIP1 expression in established T-ALL cell lines has a negative effect on cell proliferation, which is associated with a down-regulation of COX20 and reduction in mitochondrial respiration. This indicates a dual role for PSIP1 in T-ALL, where PSIP1 acts as a tumor suppressor in leukemia initiation but acts as a dependency factor in leukemia maintenance.

RESULTS

Recurrent loss-of-function *PSIP1* mutations in patients with T-ALL

To investigate the role of PSIP1 in T-ALL, we first performed a detailed expression analysis of *PSIP1* in T-ALL by using publicly available T-ALL patient data (*19*–*22*). Compared to normal T cells, a significant decrease in *PSIP1* mRNA levels was observed in all T-ALL subtypes, except for the TLX1 subgroup (fig. S1A) (*20*). Similar variable and lower PSIP1 levels were detected on protein level when comparing three healthy thymus samples to five T-ALL patient-derived xenograft samples (fig. S1B). In addition, we integrated RNA sequencing (RNA-seq) data of an extensive study that combines transcriptomic and genomic data of 264 pediatric and young adult T-ALL patients (PeCan) (*19*, *21*, *22*) with RNA-seq data of human primary thymus samples (*23*). In this second dataset, a similar distribution of *PSIP1* mRNA expression levels was detected, with significant lower *PSIP1* mRNA levels in the LMO2/LYL1, NKX2.1, and TAL1 molecular T-ALL subgroups (Fig. 1A). *PSIP1* is encoded on the short arm of chromosome 9, a genomic region that is frequently deleted in primary T-ALL patient samples. In 13% of the PeCan T-ALL patients (34 of 264), 9p deletions that contained the *PSIP1* locus were identified (Fig. 1B, orange triangles) and those correlated with a reduction in *PSIP1* mRNA levels. In one of these patients, a second hit caused by an early frameshift mutation (Y18fs) on the remaining *PSIP1* allele resulted in full loss of *PSIP1* activity (Fig. 1B, blue square). Considering that the *PSIP1* gene is located in close proximity of *CDNK2A*, a frequently deleted gene in T-ALL (*24*), we verified that the observed deletions of *PSIP1* are not exclusively co-occurring with *CDKN2A* deletions (fig. S2). In addition, in a recent study conducted at St. Jude Children's Research Hospital (*25*), five not previously described loss-of-function stop/frame shift mutations in *PSIP1* were identified in patients with T-ALL. Collectively, these data suggest a tumor suppressor role for PSIP1 in T-ALL, which seems contradictory to its reported cancer dependency role in KMT2Ar AML (*18*).

Loss of *Psip1* accelerates T-ALL initiation in mice

To evaluate the putative tumor suppressor role of PSIP1 in T-ALL, we crossed conditional *Psip1*$^{fl/fl}$ knockout (KO) mice (*26*) with two murine spontaneous T-ALL models. First, *Psip1*$^{fl/fl}$ mice were intercrossed with the *Lck-Cre*$^{tg/+}$ *Pten*$^{fl/fl}$ (*Pten*^{Lck}) model in which T cell restricted loss of the tumor suppressor *Pten* and results in NOTCH1-independent spontaneous T-ALL formation with a median survival of 120 days (*27*, *28*). Loss of *Psip1* in the resulting *Psip1*$^{fl/fl}$;*Pten*^{Lck} (*Psip1/Pten*^{Lck}) mice significantly accelerated leukemia development in this *Pten*-null model (Fig. 2A), with a median survival of 92 days.

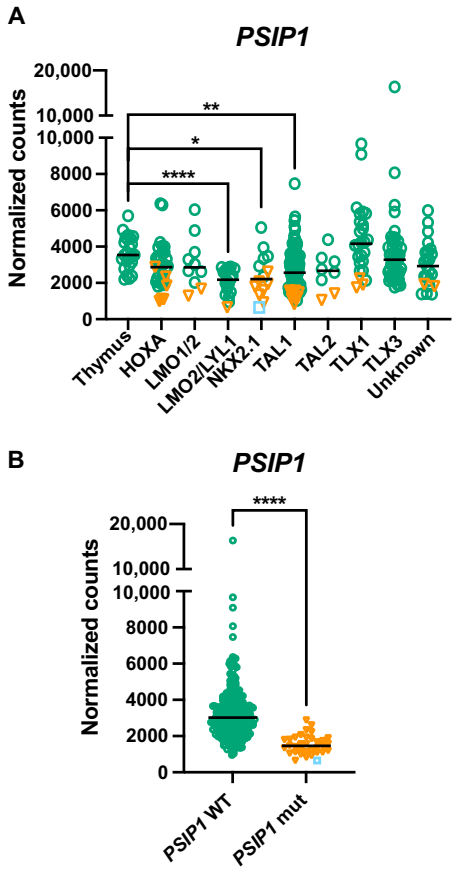

Fig. 1. *PSIP1* is lower expressed in defined T-ALL molecular subgroups and frequently deleted in patients with T-ALL. (**A**) Graph showing *PSIP1* mRNA expression in thymus and T-ALL molecular subgroups after integration of RNA-seq data from 264 patients with T-ALL (*22*) and primary human thymus samples (24 samples derived from three independent donors) (*23*). Patients with chromosomal aberration targeting the *PSIP1* locus are indicated as orange triangles, and one patient with an additional frame shift mutation (Y18fs) is indicated as a blue square (Kruskal-Wallis test with Dunn's multiple comparisons test). (**B**) *PSIP1*-deleted/mutated T-ALL cases (*PSIP1* mut) have lower expression levels of *PSIP1* compared to cases with WT *PSIP1* alleles (*PSIP1* WT) (Mann-Whitney test) (*23*). *$P < 0.05$, **$P < 0.01$, and ****$P < 0.0001$.

Moreover, we also intercrossed *Psip1*$^{fl/fl}$ mice with *CD2-Lmo2*$^{tg/+}$ mice, which develop T-ALL with two distinct patterns of gene expression, reflecting either immature/early T cell precursor (ETP) T-ALL or mature NOTCH1-driven T-ALLs (*29*). The *CD2-iCre* (*30*) was used to delete *Psip1* in the lymphoid compartment, from the common lymphoid progenitors onward. Also, in this second spontaneous T-ALL mouse model, a significant acceleration of leukemia development was observed upon the loss of *Psip1* (Fig. 2B): *Psip1*$^{fl/fl}$;*CD2-iCre*$^{tg/+}$;*CD2-Lmo2*$^{tg/+}$ (*Psip1/Lmo2*^{CD2}) had a median survival of 213 days compared to 345 days for the Cre-negative littermate control (*Lmo2*^{CD2}) mice. In both models, no differences were noted in organ infiltration or immunophenotype upon the loss of *Psip1* (table S1). Depletion of *Psip1* transcripts and PSIP1 protein was confirmed on thymic lymphoma samples from both models by quantitative reverse transcription polymerase chain reaction (RT-qPCR) (fig. S3) and by Western blot (Fig. 2C and fig. S4), respectively. To evaluate whether the acceleration in leukemia development was

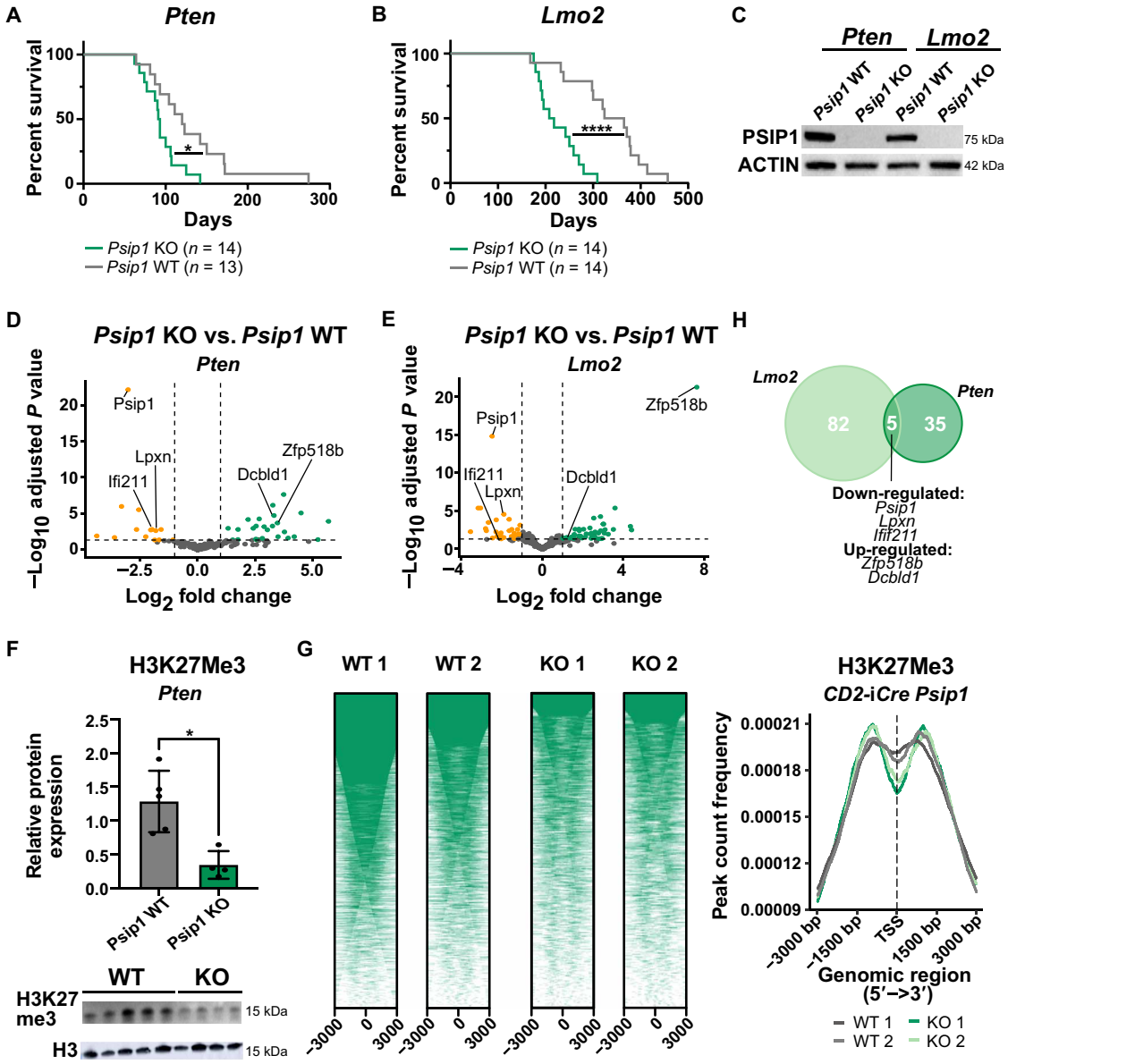

Fig. 2. A tumor-suppressive role for Psip1 in T-ALL tumor initiation. (**A** and **B**) Kaplan-Meier survival curves for mice with conditional loss of *Psip1* that were crossed with either the *Lck-Cre Pten floxed* (*Pten*) model (A) or *CD2-Lmo2*^{tg} (*Lmo2*) model (B). The resulting *Psip1* KO mice (*Psip1*$^{fl/fl}$*Lck-Cre*$^{tg/+}$*Pten*$^{fl/fl}$ or *Psip1*$^{fl/fl}$*CD2-iCre*$^{tg/+}$*CD2-Lmo2*$^{tg/+}$) significantly accelerates T-ALL development compared to *Psip1* WT (*Psip1*$^{+/+}$*Lck-Cre*$^{tg/+}$*Pten*$^{fl/fl}$ or *Psip1*$^{fl/fl}$*CD2-iCre*$^{+/+}$*CD2-Lmo2*$^{tg/+}$) (Mantel-Cox test). (**C**) Western blot validating the complete loss of *Psip1* expression in tumor samples derived from the thymus of *Psip1* KO and WT mice from both spontaneous T-ALL mouse models (*Pten* or *Lmo2*). (**D** and **E**) Differential gene expression was performed on thymic lymphoma samples of mice with and without *Psip1* expression for both the *Pten* model (D) (KO: $n = 9$; WT: $n = 6$) and the *Lmo2* model (E) ($n = 6$ in each group) (log fold change> 1; *P*adj < 0.05). (**F**) Western blot (bottom) and quantification (top) of H3K27me3 protein levels in preleukemic thymus samples of 6-week-old *Pten* mice, which are *Psip1* KO or *Psip1* WT, respectively (Mann-Whitney test). Samples were diluted 10 times for H3 Western blot to avoid overexposure. (**G**) CUT&RUN analysis for H3K27me3 binding in preleukemic thymus samples of 6-week-old *Psip1*$^{fl/fl}$*/CD2-iCre*$^{tg/+}$ (KO) or Cre-negative *Psip1*$^{fl/fl}$*/CD2-iCre*$^{+/+}$ littermate control (WT) mice ($n = 2$ for each group). Individual heatmaps (left) and metanalysis (right) of H3K27me3-binding profiles −3 and +3 kb around the transcription start site. TSS, transcription start site. (**H**) Venn diagram of differentially expressed genes upon *Psip1* KO in the *Pten*^{Lck} or *Lmo2*^{CD2} T-ALL model. Five common differentially expressed genes were identified: *Psip1*, *Zfp518b*, *Dcbld1*, *Lpxn*, and *Ifi211*. *$P < 0.05$ and ****$P < 0.0001$.

associated with changes in T cell differentiation, detailed flow cytometric analysis was performed on thymi of 42 days old mice with or without T cell–specific loss of *Psip1*. No differences were observed in thymus size or immature thymocyte fractions in Lck-Cre$^{tg/+}$ Psip1$^{fl/fl}$ compared to their WT control littermates (fig. S5). In concordance with the abovementioned transcriptomic and genomic data in human T-ALL, these murine T-ALL data are highly supportive for a tumor suppressor role for PSIP1 during the T-ALL initiation.

On the basis of previous publications (*31*, *32*), we hypothesized that PSIP1 exerts its tumor-suppressive function by facilitating DNA repair, hence that the loss of *Psip1* drives genetic instability to promote leukemia formation. Therefore, we analyzed the levels

of γH2AX, a marker for double-stranded DNA damage, on thymi from preleukemic 42-day-old *Pten*^{Lck} or *Lmo2*^{CD2} mice with or without PSIP1 KO by Western blot. However, no significant difference was observed in γH2AX protein levels in these preleukemic thymi (fig. S4).

As an alternative approach to elucidate the underlying mechanisms of this tumor suppressor role of PSIP1, we performed gene expression profiling by RNA-seq on *Psip1* KO and *Psip1* WT thymus tumor samples harvested both from the *Pten*^{Lck} and the *Lmo2*^{CD2} model. However, as both mouse T-ALL models gave rise to a heterogeneous set of T-ALL tumors, the separation in the principal components according to genotype was minimal (fig. S6). We were able to identify 40 and 87 differentially expressed genes for, respectively, the *Pten*^{Lck} and the *Lmo2*^{CD2} model (Fig. 2, D and E, and tables S2 and S3). Gene set enrichment analysis (GSEA) was performed, but no relevant gene sets passed the false discovery rate threshold of 0.25 (*33*). Nevertheless, an enrichment for EZH2 target genes and H3K27 trimethylated genes was found in Enrichr (*34*) for both mouse models (fig. S7). EZH2 is a core subunit of the Polycomb repressive complex 2 (PRC2), which acts as an H3K27me3 methyl transferase. Although no difference was detected in EZH2 expression levels, a global down-regulation of H3K27me3 was detected in preleukemic thymi of *Psip1*/*Pten*^{Lck} mice. This observation could not be confirmed in the *Lmo2*^{CD2} model (Fig. 2F and fig. S8). To get a better understanding whether PSIP1 modulates H3K27me3 signaling, we performed quantitative spike-in controlled CUT&RUN for H3K27me3 on murine thymi with or without *Psip1* expression (*Psip1*$^{fl/fl}$;*CD2*-i*Cre*$^{tg/+}$ or *Psip1*^{CD2}). Less peaks for H3K27me3 were detected in thymi of mice without *Psip1* expression compared to WT mice (Fig. 2G, fig. S9, and tables S4 and S5). In addition, we evaluated whether common differentially expressed genes could be found to identify targets that are downstream affected by *Psip1* loss, independent of the type of T-ALL. Five common differential expressed genes were detected: *Psip1*, *Dcbld1*, *Lpxn*, and *Ifi211* and the gene coding for the EZH2 interacting factor *Zfp518b* (Fig. 2H) (*35*, *36*). In conclusion, our data demonstrate a tumor-suppressive role for PSIP1 in T-ALL initiation, and our molecular analysis correlates it to the modulation of H3K27me3 signaling.

Down-regulation of PSIP1 in T-ALL cell lines has a negative effect on cell proliferation in vitro

This tumor-suppressive role of PSIP1 in T-ALL initiation seems in part contradictory to the previously published and publicly available results demonstrating that PSIP1 is a dependency factor for KMT2Ar leukemias (*13*, *17*, *18*). To further examine the role of PSIP1 in T-ALL tumor maintenance, we conducted knockdown experiments of PSIP1 in several human T-ALL cell lines, which have different KMT2Ar mutational states and represent different T-ALL subtypes. An efficient knockdown was achieved upon lentiviral transduction, using vectors that contained two independent short hairpin RNAs (shRNAs) targeting *PSIP1* (shPSIP1 1 and shPSIP1 2) and a green fluorescent protein (GFP) reporter (Fig. 3A). In vitro competitive proliferation assays were performed for which these cells with PSIP1 knockdown and GFP expression were mixed with an equal number of cells transduced with a scrambled short hairpin containing a blue fluorescent protein (BFP) reporter (shCtrl BFP). The ratio of GFP/BFP, which is a robust measure for the effect of the hairpins on cellular proliferation, was assessed over time by flow cytometry (Fig. 3B). As an additional control, a similar mix of cells was made with scrambled hairpins containing either a GFP or BFP reporter (shCtrl). As a proof of principle for our experimental setup, an KMT2Ar AML cell line, Molm-13, was tested. As described before, the loss of *PSIP1* expression had a negative effect on AML cell proliferation (Fig. 3C) (*18*). Also in five tested T-ALL cell lines, PSIP1 down-regulation led to a significant decrease in proliferation (Fig. 3, D to H). Furthermore, this antiproliferative effect was independent of the presence of a KMT2A rearrangement or T-ALL subtype. However, KMT2Ar cell lines (Karpas-45 and Molm-13) seem more sensitive to the loss of PSIP1 expression based on how rapid they were overgrown by the shCtrl BFP control cells. To better understand this difference, an annexin–7-Aminoactinomycin D (7AAD) staining was performed to quantify the number of apoptotic cells. In KMT2Ar cell lines (Molm-13 and Karpas-45), the loss of PSIP1 induced apoptosis, while this is not the case in non-KMT2Ar cell lines (Jurkat and Loucy) (Fig. 3I).

Next, we aimed to rule out the possibility that the observed dual role of PSIP1 in T-ALL is attributable to species-specific differences (mouse versus human T-ALL) or variations in growth conditions (in vivo versus in vitro). To address a potential species bias, we also evaluated the effects of *Psip1* knockdown in a murine T-ALL cell line, derived from a *Pten*^{Lck} thymic lymphoma (Fig. 4A). Similar to the experimental setup depicted in Fig. 3B, a competitive proliferation assay was performed with short hairpins targeting murine *Psip1* expression. Although the knockdown by the second hairpin only led to a 25% reduction of PSIP1 protein level, a consistent and significant decrease in proliferation of the murine T-ALL cell line was observed, analogous to the effect seen in human T-ALL cell lines (Fig. 4B). In addition, to negate that the dual role is due to in vitro and in vivo difference, we successfully cloned and validated the previously used shRNA targeting human *PSIP1* in a doxycycline-inducible vector in Jurkat cells (fig. S10). Immunocompromised NOD-*Prkdc*^{scid}-*IL2rg*^{Tm1}/Rj (NXG) mice were engrafted with one million Jurkat cells, which were transduced with either a control hairpin (shCtrl) or a hairpin targeting *PSIP1* (shPSIP1 2) (Fig. 4C). Five days postinjection, mice were switched from normal (control) to doxycycline-containing food. As a control for the effect of doxycycline on T-ALL maintenance, a group of shCtrl mice was kept on control food lacking doxycycline. If one of the mice reached a humane endpoint, then all mice were euthanized, and bone marrow cells were collected to measure the percentage human CD45-positive cells. Doxycycline did not influence the development of T-ALL (Fig. 4D). Knockdown of *PSIP1* led to a reduced leukemic burden as indicated by a significant lower percentage of hCD45-positive leukemic cells in the bone marrow of these mice. These results indicate that PSIP1 also acts as a dependency factor in an in vivo setting (Fig. 4D).

Down-regulation of PSIP1 is linked to a loss of COX20 expression

Considering that *PSIP1* knockdown in the non-KMT2Ar cell line Jurkat severely reduced proliferation without the induction of apoptosis or impairment of cell cycle (Fig. 3, E and I, and fig. S11), we wanted to further investigate the underlying molecular mechanisms. To get an insight on the downstream targets of PSIP1, we performed CUT&RUN to see where PSIP1 binds to in the genome. As described previously (*6*), PSIP1 primarily binds close to transcription start sites (fig. S12). Unexpectedly, no enrichment was observed for KMT2A target genes, but instead a strong enrichment for ALF Transcription Elongation Factor 4 (AF4) and ENL was

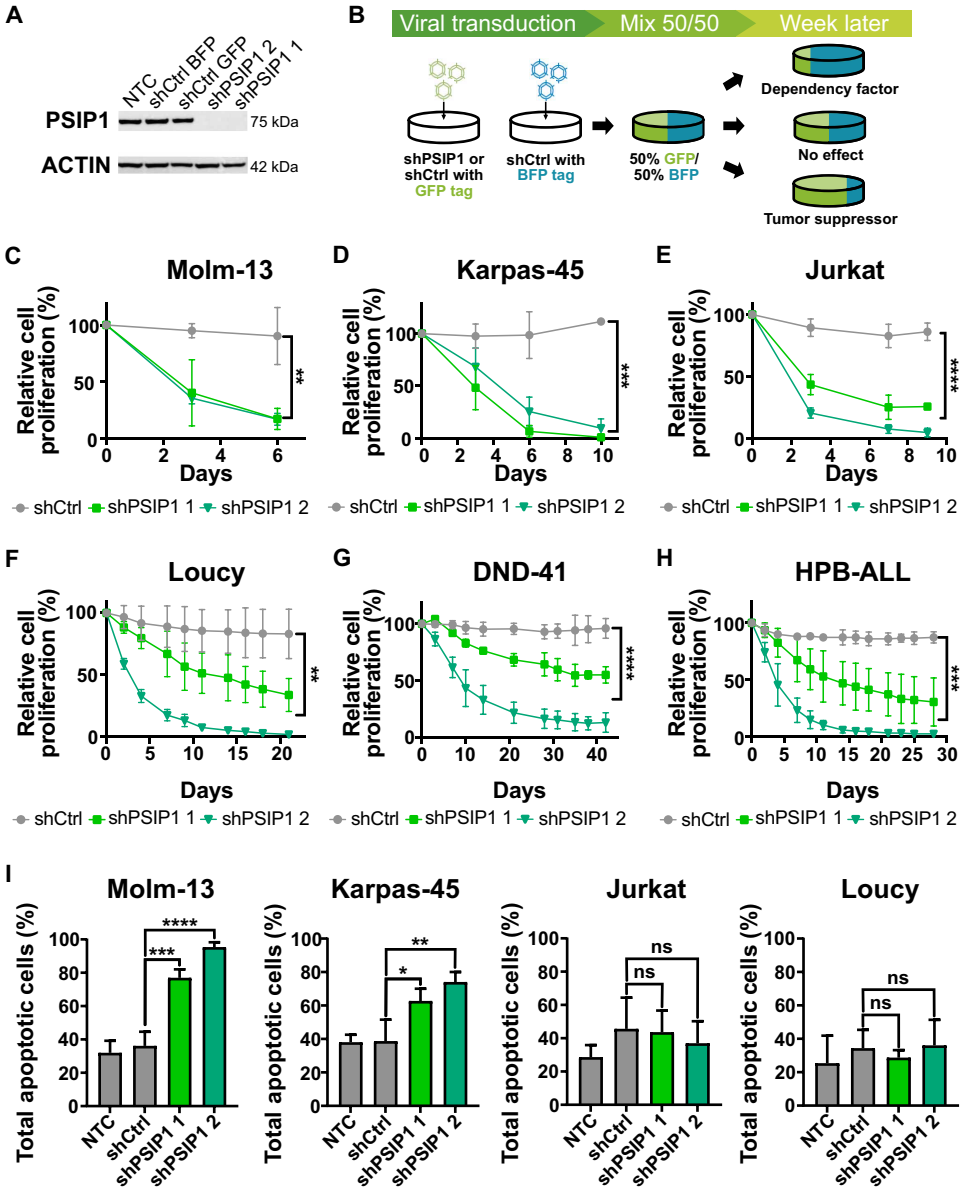

Fig. 3. PSIP1 acts a dependency factor in T-ALL tumor maintenance. (**A**) Validation of the knockdown of PSIP1 in Jurkat on protein level via Western blot. (**B**) Schematic representation of the in vitro proliferation assay. Cells are transduced with hairpins containing a GFP tag, which were either targeting PSIP1 (shPSIP1 1 and shPSIP1 2) or a scrambled control hairpin (shCtrl GFP). Those cells are then mixed in a 50/50 ratio with cells that were transduced with a BFP-tagged control hairpin (shCtrl BFP). Afterward, proliferation was assessed by flow cytometry. (**C**) The assay was validated using a KMT2Ar AML cell line, Molm-13, where loss of PSIP1 led to an impaired proliferation rate [$n = 3$, repeated measures two-way analysis of variance (ANOVA) with Geisser-Greenhouse correction]. A similar phenotype was observed in five different T-ALL cell lines, Karpas-45 (**D**), Jurkat (**E**), Loucy (**F**), DND-41 (**G**), and HPB-ALL (**H**), and was independent of the T-ALL subtype or the presence of an KMT2Ar ($n = 3$, repeated measures two-way ANOVA with Geisser-Greenhouse correction). (**I**) Annexin-7AAD stainings demonstrate that loss of PSIP1 expression induces apoptosis in KMT2Ar cell lines (Molm-13 and Karpas-45), while this is not observed in non-KMT2Ar cell lines (Jurkat and Loucy) ($n = 3$, time point: 6 days, one-way ANOVA with Dunnett's multiple comparisons test). NTC, nontransduced control; ns, not significant. *$P < 0.05$, **$P < 0.01$, ***$P < 0.001$, and ****$P < 0.0001$.

detected, which are frequently found to be fusion partners of KMT2A (Fig. 5A). In addition, transcriptome profiling by RNA-seq was conducted 72 hours after knockdown of *PSIP1* in Jurkat cells. A total of 80 differentially expressed genes were detected (Fig. 5B and table S6). Notably, we did not observe the down-regulation of *HOXA* genes and other well-known MLL target genes as described upon PSIP1 loss in AML cell lines (*10*–*12*). Instead, GSEA (*33*) did show a negative enrichment of the mitochondrial cytochrome C oxidase assembly upon knockdown of *PSIP1* (Fig. 5C). Cytochrome C oxidase is a major complex in the respiratory chain of the mitochondria, which is important in oxidative phosphorylation as it is the terminal step in the mitochondrial electron transfer chain (*37*). The "cytochrome C oxidase assembly factor 20" (COX20) was found to be significantly down-regulated in Jurkat upon loss of *PSIP1* expression (Fig. 5D). Considering that the loss of *COX20* in human embryonic kidney (HEK) 293T was previously reported to lead to

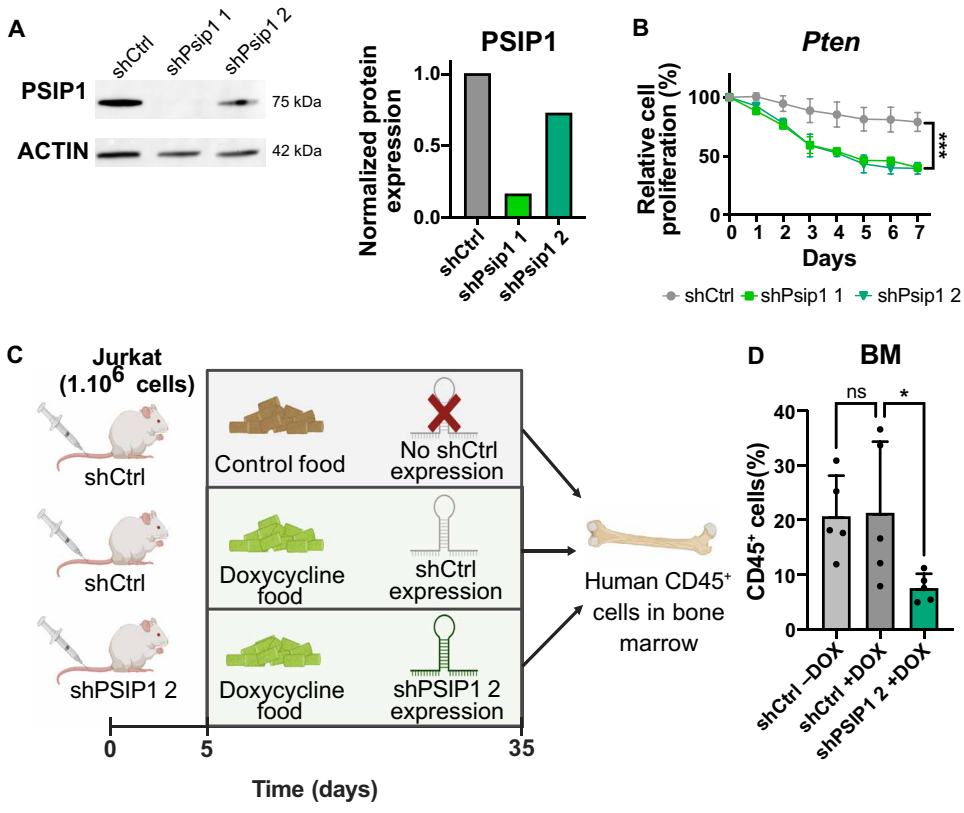

Fig. 4. PSIP1 acts as a dependency factor in a murine-derived T-ALL cell line and T-ALL maintenance in vivo. (**A**) Western blot analysis (left) and quantification (right) of PSIP1 and ACTIN (loading control) in a murine *Pten*$^{fl/fl}$;*Lck-Cre*$^{tg/+}$ (*Pten*) cell line that was transduced with a scrambled control hairpin or hairpins targeting murine *Psip1*. The PSIP1 levels normalized against house-keeping gene β-ACTIN. (**B**) Loss of *Psip1* expression also had a negative effect on the cell proliferation rate of a murine *Pten* cell line ($n = 3$, two-way ANOVA). (**C**) Schematic representation of the conducted in vivo experiment. Immunocompromised NXG mice were engrafted with one million of Jurkat cells that were either transduced with a doxycycline-inducible control hairpin (shCtrl) or a hairpin targeting *PSIP1* (shPSIP1 2). After 5 days, mice were switched to doxycycline-containing food or maintained on control food. Thirty days after the start of doxycycline treatment, the mice were euthanized, and the percentage of hCD45$^+$ leukemic cells was analyzed (created in BioRender). (**D**) Doxycycline-inducible knockdown of *PSIP1* (shPSIP1 2) led to lower levels of hCD45-positive cells in the bone marrow (BM) compared to control mice (shCtrl) ($n = 5$, Kruskal-Wallis test with Dunn's multiple comparisons test). *$P < 0.05$ and ***$P < 0.001$.

lower endogenous cell respiration and lower cytochrome c oxidase activity, we hypothesized that the slower proliferation rate upon *PSIP1* expression loss might be driven by this down-regulation of *COX20* (*38*). To further establish this down-regulation of *COX20*, we validated the mRNA expression levels of *COX20* by RT-qPCR in two KMT2Ar (Molm-13 and Karpas-45) and two non-KMT2Ar (Jurkat and Loucy) upon *PSIP1* knockdown (Fig. 5E and fig. S13). Furthermore, the down-regulation of *COX20* in these cell lines was also validated at the protein level (Fig. 5F and fig. S14). Within the CUT&RUN data, some binding of PSIP1 at the *COX20* locus could be observed (fig. S15). Independently of the presence of a KMT2A rearrangement or T-ALL subtype, a clear down-regulation of *COX20* expression was observed upon the loss of *PSIP1* expression.

COX20 loss impairs T-ALL cell line proliferation and phenocopies PSIP1 loss

To demonstrate that the down-regulation of *COX20* may be responsible for the observed decrease in proliferation upon the loss of PSIP1, an in vitro competitive proliferation assay, similar to described in Fig. 3B, was performed using short hairpins targeting *COX20* (Fig. 6A). In both the KMT2Ar and non-KMT2Ar cell lines, Karpas-45 and Jurkat, respectively, a decrease in proliferation was detected upon knockdown of *COX20* (Fig. 6, B and C). Equivalently to the observed effect upon knockdown of *PSIP1*, loss of *COX20* expression specifically induced apoptosis in the KMT2Ar T-ALL cell line Karpas-45, which was not seen in the non-KMT2Ar T-ALL cell line Jurkat (Fig. 6D). Since it was already previously described that *COX20* down-regulation impairs mitochondrial respiration in HEK-293T (*38*), we next evaluated whether the loss of proliferation upon knockdown of *PSIP1* could be correlated with an impairment in mitochondrial respiration. Therefore, a Seahorse XF Mito Stress test was conducted on Jurkat cells transduced with either a control hairpin or hairpins targeting PSIP1. As a positive control for the assay, a hairpin targeting *COX20* was taken along. Loss of PSIP1 led to a significant reduction of the maximal respiration of the cells (Fig. 6E).

To summarize, we have demonstrated that down-regulation of *COX20* induces an antiproliferative phenotype similar to that of *PSIP1* down-regulation. Similar to COX20 loss, reduction of PSIP1 levels leads to an impairment of mitochondrial respiration.

DISCUSSION

PSIP1 plays a critical role in the recruitment of elongation factors to the KMT2A complex in KMT2Ar AML, which was demonstrated to

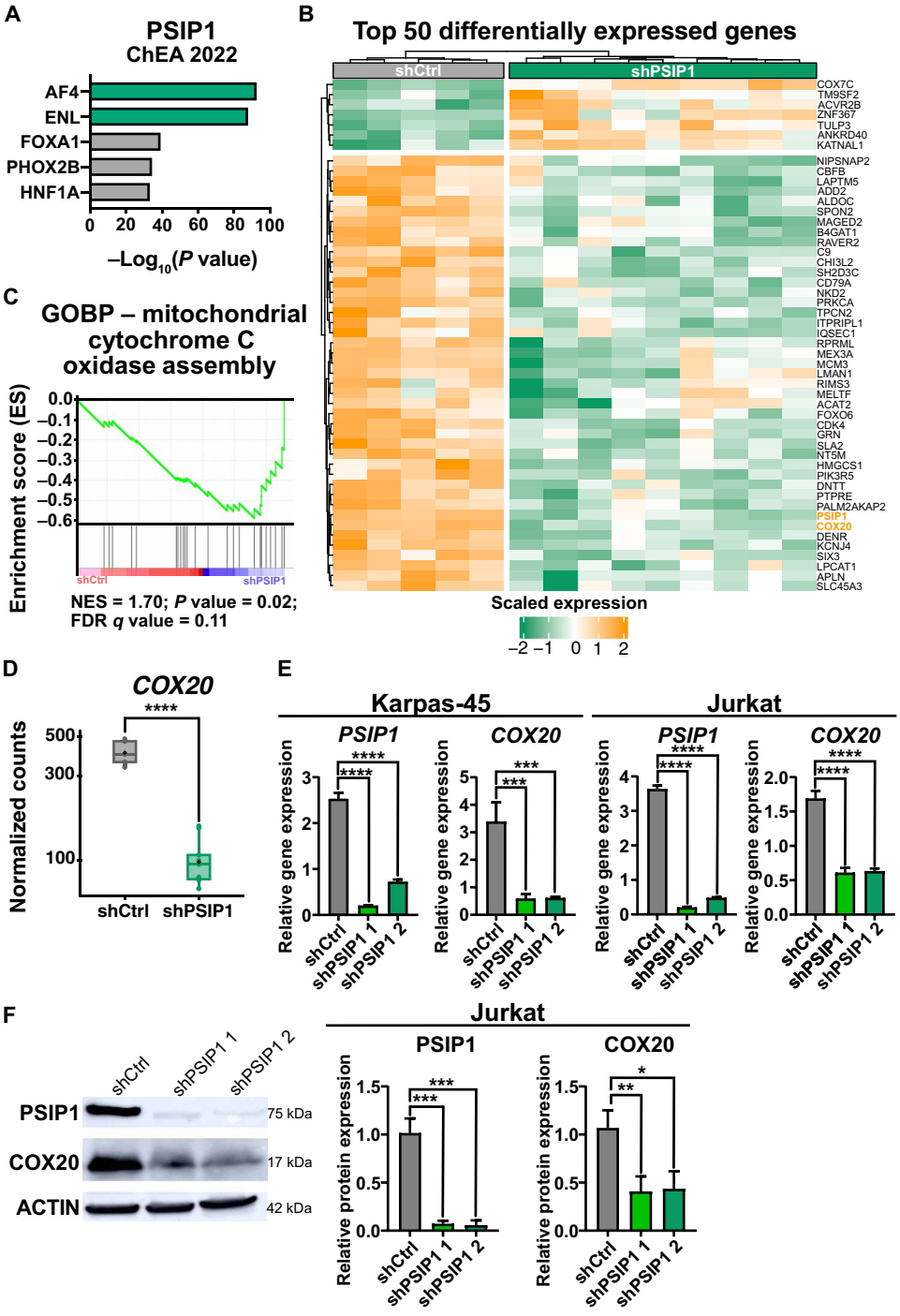

Fig. 5. COX20 is downstream regulated by PSIP1. (**A**) Enrichment for AF4 and ENL targets (ChEA2022) in the genes identified in CUT&RUN analysis for PSIP1 binding in Jurkat. (**B**) Heatmap representing the top 50 differentially expressed genes upon *PSIP1* knockdown in Jurkat ($n = 5$, time: 72 hours). (**C**) GSEA enrichment plot shows a negative enrichment for the assembly of cytochrome c oxidase upon knockdown of *PSIP1* expression in Jurkat. FDR, false discovery rate; GOBP, Gene ontology biological process; NES, normalized enrichment score. (**D**) Normalized counts for *COX20* from RNA-seq data that were described in (B). *COX20* is severely down-regulated upon down-regulation of *PSIP1* expression. (**E**) RT-qPCR for *PSIP1* and *COX20* upon *PSIP1* knockdown in Karpas-45 and Jurkat cells ($n = 3$, one-way ANOVA with Dunnett's multiple comparisons test). (**F**) Western blot validation of COX20 down-regulation on protein level in Jurkat (one blot representative for three replicates, normalization: $n = 3$, one-way ANOVA with Dunnett's multiple comparisons test). *$P < 0.05$, **$P < 0.01$, ***$P < 0.001$, and ****$P < 0.0001$.

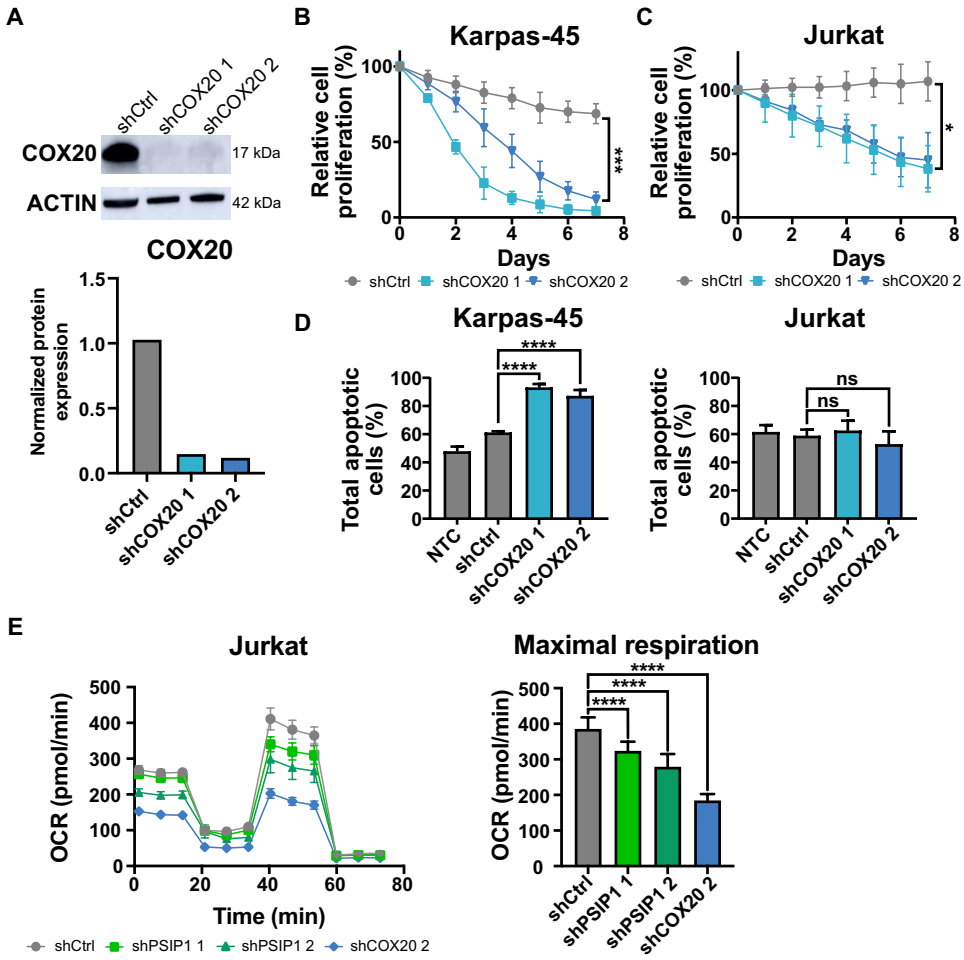

Fig. 6. COX20 is a dependency factor in T-ALL. (**A**) Western blot analysis (top) and quantification (bottom) of COX20 and Actin (loading control) levels upon knockdown of *COX20* in Jurkat at 72 hours. (**B** and **C**) In vitro proliferation assays, in Karpas-45 (B) and Jurkat (C), demonstrate that loss of *COX20* expression has a negative effect on cell proliferation rate ($n = 3$, two-way ANOVA). (**D**) Similar to the knockdown of *PSIP1*, annexin-7AAD stainings demonstrate that loss of *COX20* expression in a cell line with a KMT2Ar (Karpas-45) induces apoptosis, while this is not the case for a non-KMT2Ar cell line (Jurkat) ($n = 3$, time: 8 days, one-way ANOVA with Dunnett's multiple comparisons test). (**E**) Knockdown of PSIP1 in Jurkat reduces maximal respiration in a Seahorse XF Cell Mito Stress test ($n = 9$ technical replicates, one-way ANOVA with Dunnett's multiple comparisons test). Oxygen consumption rate (OCR) with the sequential injections of oligomycin A, carbonyl cyanide *p*-trifluoromethoxyphenylhydrazone, and antimycin A + rotenone (left) and the maximal respiration plotted separately (right). *$P < 0.05$, ***$P < 0.001$, and ****$P < 0.0001$.

be indispensable for the initiation of this type of leukemia (*6*, *18*). In T-ALL, our findings present a more complex and disease stage–specific picture of the functioning of PSIP1, with PSIP1 acting as a tumor suppressor during tumor initiation and as a dependency factor in established T-ALL cell lines. These seemingly contradictory phenotypes can be explained by two mutually exclusive mechanisms of action.

On the one hand, we were able to link the tumor suppressor function of PSIP1 to altered H3K27me3 landscape. H3K27me3 is a repressive histone mark that can be deposited by the PRC2 complex (*39*). CRISPR screens revealed a codependency between core members of the PRC2 complex (*EED* and *EZH2*) and the KMT2A complex (*PSIP1* and *Menin*), and a 57% overlap in downstream affected genes between a *PSIP1* KO and *EED* KO was detected (*40*). Almost half of the differentially expressed genes upon *PSIP1* KO were under the control of bivalently regulated promotors, which contain both the repressive H3K27me3 and the activating H3K4me3 histone mark (*40*). Similarly to PSIP1, EZH2 has been described to have a dual role in AML dependent on the disease stage. EZH2 was demonstrated to function as tumor suppressor during tumor initiation and as facilitator in established AML (*41*). The tumor-suppressive role of EZH2 could as well be linked to derepression of bivalent promotors of specific oncogenes through the loss of H3K27me3 binding. Noteworthy, *PSIP1* expression levels are higher in patients with *TLX1*-mutated T-ALL compared to other T-ALL subtypes. Although mutations targeting components of the PRC2 complex are widely prevalent in T-ALL, *TLX1* events and PRC2 mutations have been described to be mutually exclusive (*42*). Therefore, collectively with our murine data, we propose a tumor-suppressive role for PSIP1 in T-ALL through safeguarding of proper H3K27me3 occupancy.

Contrary to the previously described dependency role of PSIP1 in KMT2Ar AML, we did not observe differential expression of typical KMT2Ar target genes, for example, *HOX* genes (*6*, *18*), upon *PSIP1* knockdown in T-ALL cell lines. Instead, we identified *COX20* as a downstream affected gene. COX20 is important in the assembly of cytochrome C oxidase (complex IV) of the respiratory chain of the mitochondria. *COX20* mutations have been described to have a

causal role in patients with complex IV deficiency, which is associated with ataxia and muscle hypotonia (*43, 44*). Loss of *COX20* leads to reduced complex IV formation and consequently a reduced mitochondrial respiration (*38*). Our data indicate that the down-regulation of *COX20* upon *PSIP1* down-regulation is independent of the *KMT2A* mutational status. However, KMT2Ar cells have a higher sensitivity for the loss of *COX20*, similarly to the loss of *PSIP1*. KMT2A/MLLT3 (MLL/AF9) rearranged AML cell lines have a higher dependency on oxidative phosphorylation and therefore were more sensitive to Metformin, a complex I inhibitor, compared to non-KMT2Ar cell lines (*45*). As such, the elevated mitochondrial respiration in KMT2Ar cell lines could potentially explain the observed difference in sensitivity to *PSIP1* loss based on KMT2A mutational status. Although our study uncovered a link between PSIP1 and COX20, further research will be necessary to elucidate the exact mechanism of regulation.

PSIP1 has two different isoforms, p75 and p52, which both can recognize H3K36me3 through their N-terminal PWWP domain (*5*). Via distinct molecular mechanisms, both isoforms were previously reported to be involved in *KMT2A* and *HOX* genes regulation in AML (*6*, *13*, *18*). Considering that the observed loss-of-function mutations in patients with T-ALL affect both isoforms, we decided to use in vivo and in vitro models in which both isoforms are down-regulated simultaneously. Therefore, further research will need to be conducted to identify potential isoform-specific differences.

In summary, our data demonstrate a disease phase-dependent role of the epigenetic factor PSIP1 in T-ALL, a tumor suppressor gene during leukemia initiation and a dependency factor in leukemia maintenance (Fig. 7). Considering that PSIP1 is dispensable for normal hematopoiesis (*18*) and has a compartmentalized function based on the disease phase suggests that pharmacological targeting of PSIP1 could be a viable therapeutic strategy to target all patients with T-ALL, independent of the molecular and genetic subgroup.

MATERIALS AND METHODS

Primary samples

Thymocytes were obtained from the Universitair Ziekenhuis (UZ) Ghent hospital via an established ethical protocol. Primary T-ALL cells (samples DFAT27681, CBAT93917, DFAT-72032, CBAT-27299, and DFAT-53836) were purchased from the "Public Repository of Xenografts" (PRoXe, Dana-Farber Cancer Institute, Boston, MA) under an established material transfer agreement. Cells were propagated via NXG mice (NOD-Prkdcscid-II2rgtm1/Rj, Janvier, Saint-Berthevin, France) and isolated from the spleens for downstream analyses.

Murine T-ALL models

Conditional *Psip1* KO mice (*Psip1*$^{fl/fl}$) (*26*) harbor loxP sites flanking exon 3 of *Psip1*, enabling restricted KO of both *Psip1* isoforms. These mice were crossed with two murine T-ALL models, the *Lck-Cre*$^{tg/+}$ *Pten*$^{fl/fl}$ and the *CD2-iCre*$^{tg/+}$ *CD2-Lmo2*$^{tg/+}$ models (*28*, *29*). For both models, mice with and without PSIP1 expression were monitored for leukemia development. Survival percentages were plotted using a Kaplan-Meier survival curve, and statistical differences were determined using the log-rank Mantel-Cox test. All animal experiments were approved by Ethical Committee for animal experimentation of the Faculty of Medicine and Health Sciences of Ghent University and Ghent University Hospital.

Collection of mouse samples

Tumors were collected, dissociated into a single-cell suspension by using a 40-μm cell strainer (Novolab, A09360), treated with red blood cell lysis buffer (Gibco, A1049201), washed in phosphate-buffered saline (PBS) (Gibco, 10010023), and stored as a pellet and/or viable cells in 10% dimethyl sulfoxide in heat-inactivated fetal bovine serum (FBS) (HyClone GE, SV3016003).

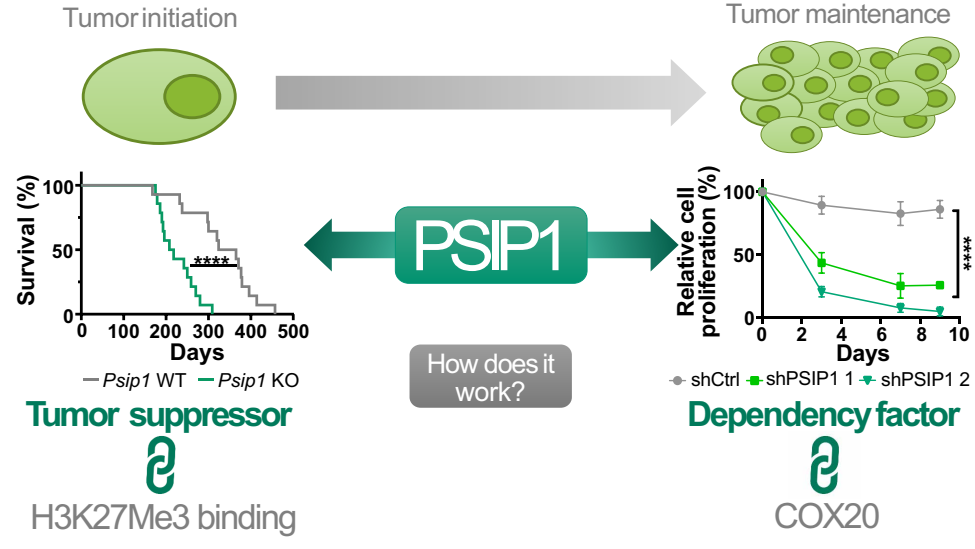

Fig. 7. Graphical abstract: Dual role of the epigenetic factor PSIP1 in T-ALL. Loss-of-function mutations in patients with T-ALL in combination with an accelerated leukemic onset in two conditional *Psip1* KO mouse models indicate a tumor-suppressive role for PSIP1 role in the onset of T-ALL. In addition, we propose safeguarding proper H3K27me3 occupancy as a mechanism of action for PSIP1 its tumor-suppressive function. During leukemia maintenance, we established that down-regulation of *PSIP1* has a negative effect on T-ALL proliferation which is independent of *KMT2A* mutational status and T-ALL subtype. Furthermore, we were able to functionally link the observed phenotype to a reduced mitochondrial respiration orchestrated by down-regulation of *COX20*. ****$P < 0.0001$.

Plasmids

shRNAs targeting *PSIP1* and *COX20* and the according nontargeting control hairpin were acquired from Sigma-Aldrich [Mission The RNAi Consortium (TRC) vectors]. The puromycin cassette was swapped with a GFP or BFP reporter by restriction of the Bam HI and Kpn I (TRC1 vector backbone) or Sex AI (TRC2 vector backbone). The sequences of the shRNAs are described in table S7.

Cell lines

Molm-13, Jurkat, Loucy, HPB-ALL, DND-41, and HEK-293T were purchased from the German Collection of Microorganisms and Cell Cultures, and Karpas-45 was purchased from the European Collection of Authenticated Cell Cultures. The human cell lines were cultured in RPMI 1640 medium (Gibco, 52400025) supplemented with 10% (Jurkat, Loucy, DND-41, and HEK-293T) or 20% (Molm-13, Karpas-45, and HPB-ALL) FBS, penicillin (100 U/ml) and streptomycin (100 μg/ml) (Gibco, 15140163), and 2 mM L-glutamine (L-Glu) (Gibco, 25030081) at 37°C and 5% CO_2.

A primary murine T-ALL cell line was derived from a thymoma of an *Lck-Cre*$^{tg/+}$ *Pten*$^{fl/fl}$ *Psip1*$^{fl/fl}$ mouse using a previously described protocol (*46*). Concisely, the thymoma was dissected and cut in smaller pieces using two scalpel blades, and tumor cells/clumbs were collected in RPMI 1640 medium containing 15% FBS, penicillin (100 U/ml) and streptomycin (100 μg/ml), 2 mM L-Glu, 0.1 mM nonessential amino acids (Gibco, 11140050), 10 mM β-mercaptoethanol (Thermo Fisher Scientific), and recombinant murine interleukin-7 (mIL-7; 5 ng/ml) (Peprotech, 217-17) and cultured at 37°C and 5% CO_2. The cells were split three times a week and became independent of mIL-7 after 3 weeks.

Lentiviral transduction

Lentiviral particles were produced by cotransfection of the shRNA TRC vector, pMD2.G and psPAX2 into HEK-293T cells using jetPEI (Polyplus, 101000020). Forty-eight hours posttransfection, the culture medium containing the lentiviral particles was collected. Human and murine cell lines were transduced with these viral particles by spinoculation (2300 rpm, 90 min, 32°C) in the presence of polybrene (8 μg/ml; Sigma-Aldrich, H9268). Transduction efficiency was verified by flow cytometry (LSR II Flow Cytometer or LSRFortessa Cell Analyzer, BD Biosciences) by the GFP or BFP reporter. If the efficiency was below 80%, then the cells were fluorescence-activated cell sorting (FACS)–sorted using a FACSAria III Cell Sorter (BD Biosciences).

In vitro competitive proliferation assay

Cells were transduced using vectors that contain shRNAs, targeting either PSIP1 (shPSIP1), COX20 (shCOX20), or nothing (shCtrl), with a GFP reporter. These cells were mixed in 50/50 ratio with cells transduced with a scrambled shRNA vector containing a BFP reporter (shCtrl BFP), serving as an internal control for proliferation. The ratio of GFP/BFP was assessed over time by flow cytometry (LSR II Flow Cytometer, BD Biosciences). A graphic illustration of the experimental setup can be found in Fig. 3B.

Immunoblot

Cells were lysed at a density of 1 million/ml in 1% SDS in 10 mM tris-HCl (pH 7.6) for 10 min at 95°C. Nucleic acids were removed from the lysate by addition of Benzonase Nuclease (Sigma-Aldrich, E8263). The protein content of the lysates was quantified using Pierce BCA Protein Assay (Thermo Fisher Scientific, 23225) to assure equal sample loading. A total of 10% or 8 to 16% Mini-PROTEAN TGX Precast Protein Gels (Bio-Rad, 4561035 and 4561103) were run at a constant voltage of 100 V for 90 min. Thereafter, the proteins were transferred onto nitrocellulose membranes (Bio-Rad, 1620233) at 100 V for 1 hour. The immunoblots were blocked in 5% milk powder in 1× tris-buffered saline buffer with 0.1% Tween 20 buffer before incubation with a primary antibody. The following antibodies were used: PSIP1 (1:1000; Bethyl, A300-848A), COX20 (1:1000; Proteintech, 25752-1-AP), γ-H2AX (1:1000; Bethyl, A300-081A), H3K27me3 (1:1000; Millipore, 07-449), EZH2 (1:1000; Cell Signaling Technology, 4905), β-actin (1:10,000; Proteintech, 66009-1-Ig), H3 (1:10,000; Abcam, ab1791), and horseradish peroxidase–linked secondary antibodies (1:10,000; Cell Signaling Technology, 7076S and 7074S). The immunoblots were imaged by chemiluminescent reaction with West Dura or West Femto (Thermo Fisher Scientific, 10220294 and 11859290, respectively) on an Amersham Imager 680 (GE Healthcare). The images were analyzed and quantified using the ImageJ software (National Institutes of Health).

Quantitative reverse transcription polymerase chain reaction

RNA was extracted from the samples by using the RNeasy Plus Micro Kit (QIAGEN, 74034) according to the manufacturer's instructions. Five hundred nanograms of RNA was reverse-transcribed by the iScript cDNA Synthesis Kit (Bio-Rad, 1708891). qPCR was performed with the SsoAdvanced Universal SYBR Green Supermix (Bio-Rad, 1725275) under standard PCR conditions on a LightCycler 480 System (Roche). The primers are listed in table S8. The data were normalized and analyzed in the QBase+ software (CellCarta).

Cell cycle analysis and apoptosis assay

For cell cycle analysis, cells were fixated and permeabilized in 70% ice cold ethanol (1 hour at −20°C). Afterward, the pelleted cells were washed with PBS before ribonuclease A (RNase A) treatment (0.5 mg/ml, 1 hour at 37°C; QIAGEN, 19101). Thereafter, the samples were stained by propidium iodide (40 μg/ml; BD Biosciences, 556463). For the apoptosis assay, the phycoerythrin (PE) Annexin V Apoptosis Detection Kit I (BD Biosciences, 559763) was used according to the manufacturer's instructions. Stained samples were measured on flow cytometry (LSR II Flow Cytometer or LSRFortessa Cell Analyzer, BD Biosciences).

Doxycycline-inducible viral vectors and in vivo experiment

shRNAs were cloned into the doxycycline-inducible pLKO-TET-ON vector, as previously described (*47*). For the in vitro validation of the system, Jurkat cells were treated 72 hours with doxycycline (1 μg/ml; D9891-5G, Merck). For the in vivo experiment, 15 NOD-*Prkdc*^{scid}-*IL2rg*^{Tm1}/Rj (NXG) mice (Janvier) were injected with one million Jurkat cells that were either transduced with a control shRNA (shCtrl) or a shRNA targeting human *PSIP1* (shPSIP1 2) (Fig. 4C). Five days postinjection, mice were switched to doxycycline-containing food (TD.180625, Envigo) or maintained on control food (2918D, Envigo). If a mouse reached a human endpoint (20% weight loss or complete hind leg paralysis), all mice were euthanized, and bone marrow cells were collected. Consequently, the samples were analyzed on flow cytometry (FACS Symphony, BD Biosciences) for human CD45 (130-114-569, Miltenyi Biotec).

Data mining

We extracted RNA-seq data of patients with T-ALL, described by Liu *et al.* (*22*) from the PeCan database from the St. Jude cloud and integrated this with RNA-seq raw data of 24 thymocyte samples (*23*) (PRJNA741323), downloaded from the Sequence Read Archive. The data were normalized in R with the DESeq2 package (*48*).

RNA sequencing

RNA was extracted using the RNeasy Plus Micro Kit (QIAGEN, 74034). RNA-seq libraries were prepared with the QuantSeq 3′ mRNA-Seq Library Prep Kit FWD for Illumina (Lexogen, 015.96) according to the manufacturer's instructions. The cDNA libraries were sequenced with the NextSeq500 (High Output, 75 cycli, Illumina, 20024906). Reads were aligned to GRCh38 or GRCm39 using STAR 2.7.10 (*49*) and quantified on Gencode v44. The RUV (remove unwanted variation) package was applied on the data (*50*). Differential expressed genes were identified by DeSEQ2 (*48*) using the criteria of an absolute $\log_2$ fold change of >1 and an adjusted *P* value of <0.05. Enrichment analyses were performed with GSEA (*33*) and Enrichr (*34*). Hierarchical clustering and heatmap were generated with R ComplexHeatmap (*51*).

CUT&RUN

CUT&RUN was performed using CUTANA pA/G-MNase (Epicypher, 15-1016) according to the manufacturer's instructions except for minor adaptations. Per sample, nuclei of 0.5 M cells were extracted [20 mM Hepes-KOH (pH 7.9), 10 mM KCl, 0.1% Triton X-100, 20% glycerol 1 mM $MnCl_2$, 0.5 mM spermidine, and protease inhibitors], incubated for 10 min at 4°C on a rotator with activated concanavalin A beads, resuspended in antibody buffer [150 mM NaCl, 20 mM Hepes-KOH (pH 7.5), 2 mM EDTA, 0.5 mM spermidine, and protease inhibitors], and incubated overnight at 4°C with rotation with 1:100 dilution of antibody recognizing PSIP1 (Bethyl, A300-848A), H3K27me3 (Cell Signaling Technology, 97335), H3K36me3 (Abcam, ab9050), or a rabbit anti–immunoglobulin G (Cell Signaling Technology, 3900S). Targeted chromatin digestion and release were performed with 2.5 μl of CUTANA pA/G-MNase and 100 mM $CaCl_2$. The reaction was terminated with STOP buffer [340 mM NaCl, 4 mM EGTA, 20 mM EDTA, RNase (0.05 mg/ml), and glycogen (0.05 μg/ml)]. For the mouse samples, spike-in *Escherichia coli* DNA (0.01 ng/ml; Epicypher, 18-1401) was added. Retrieved genomic DNA was purified with the CUTANA DNA purification kit V2 (Epicypher, 14-0050). Afterward, samples were library prepped using the NEBNext Ultra II DNA Library Prep Kit according to the manufacturer's instructions, but NEBNext Endprep was conducted at 50°C for 1 hour. Sequencing was done on the AVITI, 2 × 75 (Element Biosciences). Data were processed using an in-house data analysis pipeline as previously described (*52*). In short, adapter sequences were trimmed using Trim-Galore v0.6.5, and reads were aligned to GRCh38 or GRCm39 using bowtie2 v2.3.1. Sorted and quality-filtered (MAPQ30) aligned files were deduplicated using picard v2.25.1. Peak calling was performed using MACS2 v2.1.0, and resulting significant peaks were further processed using the ChIPseeker R package (v1.38.0). In addition, the data were processed using publicly available NextFlow pipeline (https://nf-co.re/cutandrun/3.1) (*53*). Motif enrichment analysis was performed using Homer (v5.1) and MEME-ChIP (v5.5.6) (*54, 55*).

Seahorse XF96

A Seahorse XF Cell MitoStress Test (Agilent Technologies, 103015-100) was conducted on Jurkat cells 10 days after transduction with indicated shRNAs. Before the assay, the cells were washed and resuspended in Seahorse XF RPMI medium (Agilent Technologies, 103681-100) supplemented with 10 mM glucose, 1 mM puryvate, and 2 mM glutamine. Afterward, 120 000 cells per well were attached to a poly-D-lysine (Gibco, A3890401)–coated Seahorse XFe96 cell culture microplates (Agilent Technologies, 103793-100) via centrifugation (200*g*, 1 min, no brake). For the Mito Stress test, oligomycin A (port A), carbonyl cyanide *p*-trifluoromethoxyphenylhydrazone (port B), and antimycin A + rotenone (port C) were added to a final concentration in the well of 1.5, 0.5, and 0.5 μM respectively. Data were analyzed using the Wave 2.6.3 Software.

Statistical analysis

Prism 10.0 (GraphPad) or R (v4.1.3) was used for statistical analyses. Enrichment analyses were performed with GSEA (*33*) and Enrichr (*34*). Hierarchical clustering and heatmap were generated with R ComplexHeatmap (*51*).

Supplementary Materials

The PDF file includes:

Figs. S1 to S15
Tables S7 and S8
Legends for tables S1 to S6

Other Supplementary Material for this manuscript includes the following:

Tables S1 to S6

REFERENCES AND NOTES

1. S. P. Hunger, C. G. Mullighan, Acute lymphoblastic leukemia in children. *N. Engl. J. Med.* **373**, 1541–1552 (2015).
2. S. Faderl, S. O'Brien, C.-H. Pui, W. Stock, M. Wetzler, D. Hoelzer, H. M. Kantarjian, Adult acute lymphoblastic leukemia. *Cancer* **116**, 1165–1176 (2010).
3. D. I. Marks, C. Rowntree, Management of adults with T-cell lymphoblastic leukemia. *Blood* **129**, 1134–1142 (2017).
4. J. O. Eidahl, B. L. Crowe, J. A. North, C. J. McKee, N. Shkriabai, L. Feng, M. Plumb, R. L. Graham, R. J. Gorelick, S. Hess, M. G. Poirier, M. P. Foster, M. Kvaratskhelia, Structural basis for high-affinity binding of LEDGF PWWP to mononucleosomes. *Nucleic Acids Res.* **41**, 3924–3936 (2013).
5. A. Engelman, P. Cherepanov, The lentiviral integrase binding protein LEDGF/p75 and HIV-1 replication. *PLOS Phatog.* **4**, e1000046 (2008).
6. L. Zhu, Q. Li, S. H. K. Wong, M. Huang, B. J. Klein, J. Shen, L. Ikenouye, M. Onishi, D. Schneidawind, C. Buechele, L. Hansen, J. Duque-Afonso, F. Zhu, G. M. Martin, O. Gozani, R. Majeti, T. G. Kutateladze, M. L. Cleary, ASH1L links histone H3 lysine 36 dimethylation to MLL leukemia. *Cancer Discov.* **6**, 770–783 (2016).
7. A. Yokoyama, M. Cleary, The menin tumor suppressor functions as a molecular adapter that tethers LEDGF to MLL proteins in leukemogenesis. *Blood* **112**, 1795 (2008).
8. J. F. Peterson, L. B. Baughn, K. E. Pearce, C. M. Williamson, J. C. Benevides Demasi, R. M. Olson, T. A. Goble, R. G. Meyer, P. T. Greipp, R. P. Ketterling, KMT2A (MLL) rearrangements observed in pediatric/young adult T-lymphoblastic leukemia/lymphoma: A 10-year review from a single cytogenetic laboratory. *Genes Chromosomes Cancer* **57**, 541–546 (2018).
9. L. Muñoz, J. F. Nomdedéu, N. Villamor, R. Guardia, D. Colomer, J. M. Ribera, J. P. Torres, J. J. Berlanga, C. Fernández, A. Llorente, M. P. Queipo de Llano, J. M. Sánchez, S. Brunet, J. Sierra, Acute myeloid leukemia with MLL rearrangements: Clinicobiological features, prognostic impact and value of flow cytometry in the detection of residual leukemic cells. *Leukemia* **17**, 76–82 (2003).
10. Q.-F. Wang, G. Wu, S. Mi, F. He, J. Wu, J. Dong, R. T. Luo, R. Mattison, J. J. Kaberlein, S. Prabhakar, H. Ji, M. J. Thirman, MLL fusion proteins preferentially regulate a subset of wild-type MLL target genes in the leukemic genome. *Blood* **117**, 6895–6905 (2011).
11. F. Kocabas, J. Zheng, S. Thet, N. G. Copeland, N. A. Jenkins, R. J. DeBerardinis, C. Zhang, H. A. Sadek, Meis1 regulates the metabolic phenotype and oxidant defense of hematopoietic stem cells. *Blood* **120**, 4963–4972 (2012).
12. R. A. Alharbi, R. Pettengell, H. S. Pandha, R. Morgan, The role of *HOX* genes in normal hematopoiesis and acute leukemia. *Leukemia* **27**, 1000–1008 (2013).
13. A. Yokoyama, M. L. Cleary, Menin critically links MLL proteins with LEDGF on cancer-associated target genes. *Cancer Cell* **14**, 36–46 (2008).

14. S. C. Chandrasekharappa, S. C. Guru, P. Manickam, S.-E. Olufemi, F. S. Collins, M. R. Emmert-Buck, L. V. Debelenko, Z. Zhuang, I. A. Lubensky, L. A. Liotta, J. S. Crabtree, Y. Wang, B. A. Roe, J. Weisemann, M. S. Boguski, S. K. Agarwal, M. B. Kester, Y. S. Kim, C. Heppner, Q. Dong, A. M. Spiegel, A. L. Burns, S. J. Marx, Positional cloning of the gene for multiple endocrine neoplasia-type 1. *Science* **276**, 404–407 (1997).
15. A. Yokoyama, T. C. P. Somervaille, K. S. Smith, O. Rozenblatt-Rosen, M. Meyerson, M. L. Cleary, The menin tumor suppressor protein is an essential oncogenic cofactor for MLL-associated leukemogenesis. *Cell* **123**, 207–218 (2005).
16. C. Caslini, Z. Yang, M. El-Osta, T. A. Milne, R. K. Slany, J. L. Hess, Interaction of MLL amino terminal sequences with menin is required for transformation. *Cancer Res.* **67**, 7275–7283 (2007).
17. K. Čermáková, P. Tesina, J. Demeulemeester, S. El Ashkar, H. Méreau, J. Schwaller, P. Řezáčová, V. Veverka, J. De Rijck, Validation and structural characterization of the LEDGF/p75–MLL interface as a new target for the treatment of MLL-dependent leukemia. *Cancer Res.* **74**, 5139–5151 (2014).
18. S. El Ashkar, J. Schwaller, T. Pieters, S. Goossens, J. Demeulemeester, F. Christ, S. Van Belle, S. Juge, N. Boeckx, A. Engelman, P. Van Vlierberghe, Z. Debyser, J. De Rijck, LEDGF/p75 is dispensable for hematopoiesis but essential for MLL-rearranged leukemogenesis. *Blood* **131**, 95–107 (2017).
19. C. McLeod, A. M. Gout, X. Zhou, A. Thrasher, D. Rahbarinia, S. W. Brady, M. Macias, K. Birch, D. Finkelstein, J. Sunny, R. Mudunuri, B. A. Orr, M. Treadway, B. Davidson, T. K. Ard, A. Chiao, A. Swistak, S. Wiggins, S. Foy, J. Wang, E. Sioson, S. Wang, J. R. Michael, Y. Liu, X. Ma, A. Patel, M. N. Edmonson, M. R. Wilkinson, A. M. Frantz, T.-C. Chang, L. Tian, S. Lei, S. M. A. Islam, C. Meyer, N. Thangaraj, P. Tater, V. Kandali, S. Ma, T. Nguyen, O. Serang, I. McGuire, N. Robison, D. Gentry, X. Tang, L. E. Palmer, G. Wu, E. Suh, L. Tanner, J. McMurry, M. Lear, A. S. Pappo, Z. Wang, C. L. Wilson, Y. Cheng, S. Meshinchi, L. B. Alexandrov, M. J. Weiss, G. T. Armstrong, L. L. Robison, Y. Yasui, K. E. Nichols, D. W. Ellison, C. Bangur, C. G. Mullighan, S. J. Baker, M. A. Dyer, G. Miller, S. Newman, M. Rusch, R. Daly, K. Perry, J. R. Downing, J. Zhang, St. Jude cloud: A pediatric cancer genomic data-sharing ecosystem. *Cancer Discov.* **11**, 1082–1099 (2021).
20. E. Clappier, B. Gerby, F. Sigaux, M. Delord, F. Touzri, L. Hernandez, P. Ballerini, A. Baruchel, F. Pflumio, J. Soulier, Clonal selection in xenografted human T cell acute lymphoblastic leukemia recapitulates gain of malignancy at relapse. *J. Exp. Med.* **208**, 653–661 (2011).
21. X. Zhou, J. Wang, J. Patel, M. Valentine, Y. Shao, S. Newman, E. Sioson, L. Tian, Y. Liu, S. W. Brady, D. Flasch, X. Ma, Y. Liu, R. Paul, M. N. Edmonson, M. C. Rusch, C. Li, S. J. Baker, J. Easton, J. Zhang, Exploration of coding and non-coding variants in cancer using genomepaint. *Cancer Cell* **39**, 83–95.e4 (2021).
22. Y. Liu, J. Easton, Y. Shao, J. Maciaszek, Z. Wang, M. R. Wilkinson, K. McCastlain, M. Edmonson, S. B. Pounds, L. Shi, X. Zhou, X. Ma, E. Sioson, Y. Li, M. Rusch, P. Gupta, D. Pei, C. Cheng, M. A. Smith, J. G. Auvil, D. S. Gerhard, M. V. Relling, N. J. Winick, A. J. Carroll, N. A. Heerema, E. Raetz, M. Devidas, C. L. Willman, R. C. Harvey, W. L. Carroll, K. P. Dunsmore, S. S. Winter, B. L. Wood, B. P. Sorrentino, J. R. Downing, M. L. Loh, S. P. Hunger, J. Zhang, C. G. Mullighan, The genomic landscape of pediatric and young adult T-lineage acute lymphoblastic leukemia. *Nat. Genet.* **49**, 1211–1218 (2017).
23. V. Sun, M. Sharpley, K. E. Kaczor-Urbanowicz, P. Chang, A. Montel-Hagen, S. Lopez, A. Zampieri, Y. Zhu, S. C. de Barros, C. Parekh, D. Casero, U. Banerjee, G. M. Crooks, The metabolic landscape of thymic T cell development in vivo and in vitro. *Front. Immunol.* **12**, 716661 (2021).
24. H.-P. Wang, Y.-L. Zhou, X. Huang, Y. Zhang, J.-J. Qian, J.-H. Li, X.-Y. Li, C.-Y. Li, Y.-J. Lou, W.-Y. Mai, H.-T. Meng, W.-J. Yu, H.-Y. Tong, J. Jin, H.-H. Zhu, CDKN2A deletions are associated with poor outcomes in 101 adults with T-cell acute lymphoblastic leukemia. *Am. J. Hematol.* **96**, 312–319 (2021).
25. P. Pölönen, D. Di Giacomo, A. E. Seffernick, A. Elsayed, S. Kimura, F. Benini, L. E. Montefiori, B. L. Wood, J. Xu, C. Chen, Z. Cheng, H. Newman, J. Myers, I. Iacobucci, E. Li, J. Sussman, D. Hedges, Y. Hui, C. Diorio, L. Uppuluri, D. Frank, Y. Fan, Y. Chang, S. Meshinchi, R. Ries, R. Shraim, A. Li, K. M. Bernt, M. Devidas, S. S. Winter, K. P. Dunsmore, H. Inaba, W. L. Carroll, N. C. Ramirez, A. H. Phillips, R. W. Kriwacki, J. J. Yang, T. L. Vincent, Y. Zhao, P. S. Ghate, J. Wang, C. Reilly, X. Zhou, M. A. Sanders, J. Takita, M. Kato, N. Takasugi, B. H. Chang, R. D. Press, M. Loh, E. Rampersaud, E. Raetz, S. P. Hunger, K. Tan, T.-C. Chang, G. Wu, S. B. Pounds, C. G. Mullighan, D. T. Teachey, The genomic basis of childhood T-lineage acute lymphoblastic leukaemia. *Nature* **632**, 1082–1091 (2024).
26. M.-C. Shun, N. K. Raghavendra, N. Vandegraaff, J. E. Daigle, S. Hughes, P. Kellam, P. Cherepanov, A. Engelman, LEDGF/p75 functions downstream from preintegration complex formation to effect gene-specific HIV-1 integration. *Genes Dev.* **21**, 1767–1778 (2007).
27. A. M. Martelli, F. Paganelli, A. Fazio, C. Bazzichetto, F. Conciatori, J. A. McCubrey, The key roles of PTEN in T-cell acute lymphoblastic leukemia development, progression, and therapeutic response. *Cancers* **11**, 629 (2019).
28. A. Suzuki, M. T. Yamaguchi, T. Ohteki, T. Sasaki, T. Kaisho, Y. Kimura, R. Yoshida, A. Wakeham, T. Higuchi, M. Fukumoto, T. Tsubata, P. S. Ohashi, S. Koyasu, J. M. Penninger, T. Nakano, T. W. Mak, T cell-specific loss of pten leads to defects in central and peripheral tolerance. *Immunity* **14**, 523–534 (2001).
29. S. Smith, R. Tripathi, C. Goodings, S. Cleveland, E. Mathias, J. A. Hardaway, N. Elliott, Y. Yi, X. Chen, J. Downing, C. Mullighan, D. A. Swing, L. Tessarollo, L. Li, P. Love, N. A. Jenkins, N. G. Copeland, M. A. Thompson, Y. Du, U. P. Davé, LIM domain only-2 (LMO2) induces T-cell leukemia by two distinct pathways. *PLOS ONE* **9**, e85883 (2014).
30. J. de Boer, A. Williams, G. Skavdis, N. Harker, M. Coles, M. Tolaini, T. Norton, K. Williams, K. Roderick, A. J. Potocnik, D. Kioussis, Transgenic mice with hematopoietic and lymphoid specific expression of Cre. *Eur. J. Immunol.* **54**, 314–325 (2003).
31. V. Liedtke, C. Schröder, D. Roggenbuck, R. Weiss, R. Stohwasser, P. Schierack, S. Rödiger, L. Schenk, LEDGF/p75 is required for an efficient DNA damage response. *Int. J. Mol. Sci.* **22**, 5866 (2021).
32. M. Daugaard, A. Baude, K. Fugger, L. K. Povlsen, H. Beck, C. S. Sørensen, N. H. T. Petersen, P. H. B. Sorensen, C. Lukas, J. Bartek, J. Lukas, M. Rohde, M. Jäättelä, LEDGF (p75) promotes DNA-end resection and homologous recombination. *Nat. Struct. Mol. Biol.* **19**, 803–810 (2012).
33. A. Subramanian, P. Tamayo, V. K. Mootha, S. Mukherjee, B. L. Ebert, M. A. Gillette, A. Paulovich, S. L. Pomeroy, T. R. Golub, E. S. Lander, J. P. Mesirov, Gene set enrichment analysis: A knowledge-based approach for interpreting genome-wide expression profiles. *Proc. Natl. Acad. Sci. U.S.A.* **102**, 15545–15550 (2005).
34. E. Y. Chen, C. M. Tan, Y. Kou, Q. Duan, Z. Wang, G. V. Meirelles, N. R. Clark, A. Ma'ayan, Enrichr: Interactive and collaborative HTML5 gene list enrichment analysis tool. *BMC Bioinformatics* **14**, 128 (2013).
35. F. Gimeno-Valiente, Á. L. Riffo-Campos, L. Torres, N. Tarazona, V. Gambardella, A. Cervantes, G. López-Rodas, L. Franco, J. Castillo, Epigenetic mechanisms are involved in the oncogenic properties of *ZNF518B* in colorectal cancer. *Cancers* **13**, 1433 (2021).
36. V. K. Maier, C. M. Feeney, J. E. Taylor, A. L. Creech, J. W. Qiao, A. Szanto, P. P. Das, N. Chevrier, C. Cifuentes-Rojas, S. H. Orkin, S. A. Carr, J. D. Jaffe, P. Mertins, J. T. Lee, Functional proteomic analysis of repressive histone methyltransferase complexes reveals ZNF518B as a G9A regulator. *Mol. Cell. Proteomics* **14**, 1435–1446 (2015).
37. R. Ramzan, B. Kadenbach, S. Vogt, Multiple mechanisms regulate eukaryotic cytochrome C oxidase. *Cells* **10**, 514 (2021).
38. M. Bourens, A. Boulet, S. C. Leary, A. Barrientos, Human COX20 cooperates with SCO1 and SCO2 to mature COX2 and promote the assembly of cytochrome *c* oxidase. *Hum. Mol. Genet.* **23**, 2901–2913 (2014).
39. R. Margueron, D. Reinberg, The polycomb complex PRC2 and its mark in life. *Nature* **469**, 343–349 (2011).
40. C. E. Sparbier, A. Gillespie, J. Gomez, N. Kumari, A. Motazedian, K. L. Chan, C. C. Bell, O. Gilan, Y.-C. Chan, S. Popp, D. J. Gough, M. A. Eckersley-Maslin, S.-J. Dawson, P. J. Lehner, K. D. Sutherland, P. Ernst, G. M. McGeehan, E. Y. N. Lam, M. L. Burr, M. A. Dawson, Targeting Menin disrupts the KMT2A/B and polycomb balance to paradoxically activate bivalent genes. *Nat. Cell Biol.* **25**, 258–272 (2023).
41. F. Basheer, G. Giotopoulos, E. Meduri, H. Yun, M. Mazan, D. Sasca, P. Gallipoli, L. Marando, M. Gozdecka, R. Asby, O. Sheppard, M. Dudek, L. Bullinger, H. Döhner, R. Dillon, S. Freeman, O. Ottmann, A. Burnett, N. Russell, E. Papaemmanuil, R. Hills, P. Campbell, G. S. Vassiliou, B. J. P. Huntly, Contrasting requirements during disease evolution identify EZH2 as a therapeutic target in AML. *J. Exp. Med.* **216**, 966–981 (2019).
42. G. P. Andrieu, M. Kohn, M. Simonin, C. L. Smith, A. Cieslak, M.-É. Dourthe, G. Charbonnier, C. Graux, F. Huguet, V. Lhéritier, H. Dombret, S. Spicuglia, P. Rousselot, N. Boissel, V. Asnafi, PRC2 loss of function confers a targetable vulnerability to BET proteins in T-ALL. *Blood* **138**, 1855–1869 (2021).
43. L. Chen, Y. Liu, Clinical and genetic characteristics of children with COX20-associated mitochondrial disorder: Case report and literature review. *BMC Med. Genomics* **16**, 86 (2023).
44. R. Szklarczyk, B. F. J. Wanschers, L. G. Nijtmans, R. J. Rodenburg, J. Zschocke, N. Dikow, M. A. M. van den Brand, M. G. M. Hendriks-Franssen, C. Gilissen, J. A. Veltman, M. Nooteboom, W. J. H. Koopman, P. H. G. M. Willems, J. A. M. Smeitink, M. A. Huynen, L. P. van den Heuvel, A mutation in the *FAM36A* gene, the human ortholog of COX20, impairs cytochrome c oxidase assembly and is associated with ataxia and muscle hypotonia. *Hum. Mol. Genet.* **22**, 656–667 (2013).
45. L. Liu, P. K. Patnana, X. Xie, D. Frank, S. C. Nimmagadda, A. Rosemann, M. Liebmann, L. Klotz, B. Opalka, C. Khandanpour, High metabolic dependence on oxidative phosphorylation drives sensitivity to metformin treatment in MLL/AF9 acute myeloid leukemia. *Cancers* **14**, 486 (2022).
46. R. Jinadasa, G. Balmus, L. Gerwitz, J. Roden, R. Weiss, G. Duhamel, Derivation of thymic lymphoma T-cell lines from $Atm^{-/-}$ and $p53^{-/-}$ mice. *J. Vis. Exp.* e2598 (2011).
47. D. Wiederschain, W. Susan, L. Chen, A. Loo, G. Yang, A. Huang, Y. Chen, G. Caponigro, Y. Yao, C. Lengauer, W. R. Sellers, J. D. Benson, Single-vector inducible lentiviral RNAi system for oncology target validation. *Cell Cycle* **8**, 498–504 (2009).
48. M. I. Love, W. Huber, S. Anders, Moderated estimation of fold change and dispersion for RNA-seq data with DESeq2. *Genome Biol.* **15**, 550 (2014).
49. A. Dobin, C. A. Davis, F. Schlesinger, J. Drenkow, C. Zaleski, S. Jha, P. Batut, M. Chaisson, T. R. Gingeras, STAR: Ultrafast universal RNA-seq aligner. *Bioinformatics* **29**, 15–21 (2013).

50. J. R. Gerstner, J. N. Koberstein, A. J. Watson, N. Zapero, D. Risso, T. P. Speed, M. G. Frank, L. Peixoto, Removal of unwanted variation reveals novel patterns of gene expression linked to sleep homeostasis in murine cortex. *BMC Genomics* **17**, 727 (2016).
51. Z. Gu, R. Eils, M. Schlesner, Complex heatmaps reveal patterns and correlations in multidimensional genomic data. *Bioinformatics* **32**, 2847–2849 (2016).
52. B. Decaesteker, A. Louwagie, S. Loontiens, F. De Vloed, S.-L. Bekaert, J. Roels, S. Vanhauwaert, S. De Brouwer, E. Sanders, A. Berezovskaya, G. Denecker, E. D'haene, S. Van Haver, W. Van Loocke, J. Van Dorpe, D. Creytens, N. Van Roy, T. Pieters, C. Van Neste, M. Fischer, P. Van Vlierberghe, S. S. Roberts, J. Schulte, S. Ek, R. Versteeg, J. Koster, J. van Nes, M. Zimmerman, K. De Preter, F. Speleman, SOX11 regulates SWI/SNF complex components as member of the adrenergic neuroblastoma core regulatory circuitry. *Nat. Commun.* **14**, 1267 (2023).
53. P. A. Ewels, A. Peltzer, S. Fillinger, H. Patel, J. Alneberg, A. Wilm, M. U. Garcia, P. Di Tommaso, S. Nahnsen, The nf-core framework for community-curated bioinformatics pipelines. *Nat. Biotechnol.* **38**, 276–278 (2020).
54. S. Heinz, C. Benner, N. Spann, E. Bertolino, Y. C. Lin, P. Laslo, J. X. Cheng, C. Murre, H. Singh, C. K. Glass, Simple combinations of lineage-determining transcription factors prime cis-regulatory elements required for macrophage and B cell identities. *Mol. Cell* **38**, 576–589 (2010).
55. P. Machanick, T. L. Bailey, MEME-ChIP: Motif analysis of large DNA datasets. *Bioinformatics* **27**, 1696–1697 (2011).

Acknowledgments: We thank U. Davé for providing us with the CD2-Lmo2 mice. **Funding:** This work was supported by Research Foundation Flanders (FWO), Strategic Basic Research collaboration SBO-Chromatarget G0A8B24N (P.V.V. and Z.D.); Research Foundation Flanders (FWO), project grants G0F4721N (P.N.); Flanders interuniversity consortium grant BOF23/IBF/042 (S.G. and P.N.); Research Foundation Flanders (FWO), doctoral research fellowship 1190123 N (L.D.); and Research Foundation Flanders (FWO), doctoral research fellowship 1S11223N (M.Z.A.).
Author contributions: Conceptualization: L.D., F.M., S.G., and P.V.V. Data collection: L.D., F.M., B.P., B.L., L.R., and S.T. Data analysis: L.D., B.P., and I.F. Methodology: L.D., I.F., K.D., T.P., S.G., and P.V.V. Resources: M.Z.A., S.V.B., D.D., F.V.N., Z.D., J.T., T.T., and G.B. Writing—original draft: L.D., T.P., and S.G. Writing—review and editing: All authors. Supervision: P.N., Z.D., K.D., T.P., S.G., and P.V.V. Project administration: T.P. and P.V.V. Funding acquisition: S.G. and P.V.V. **Competing interests:** The authors declare that they have no competing interests. **Data and materials availability:** All data needed to evaluate the conclusions in the paper are present in the paper and/or the Supplementary Materials. Processed gene expression data and CUT&RUN motif analysis data can be found in tables S2 to S6. Raw gene expression data and CUT&RUN data are available at GEO under accession number GSE253143. The *Psip1*$^{fl/fl}$ mice can be provided by A. Engelman pending scientific review and a completed material transfer agreement. Requests for the *Psip1*$^{fl/fl}$ mice should be submitted to alan_engelman@dfci.harvard.edu.

Submitted 17 February 2024
Accepted 30 September 2024
Published 1 November 2024
10.1126/sciadv.ado6765